RADIO SCIENCE, VOL. 37, NO. 1, 1010, 10.1029/2000RS002597, 2002

Method of moments solution of volume integral equations using parametric geometry modeling

Kubilay Sertel and John L. Volakis

Radiation Laboratory, Department of Electrical Engineering and Computer Science, University of Michigan, Ann Arbor, Michigan, USA

Received 20 December 2000; revised 5 June 2001; accepted 4 September 2001; published 20 February 2002.

[1] A higher-order geometry modeling technique is presented for the solution of volume integral equations (VIEs) involving arbitrarily shaped inhomogeneous dielectric structures. Conformal basis functions defined in curved hexahedral finite elements are used to develop a moment method solution of the VIE. Results are compared with available analytical solutions, and the method is shown to deliver higher accuracy using coarser meshes as compared to partial differential equation solvers. *INDEX TERMS:* 0619 Electromagnetics: Electromagnetic theory; 0644 Electromagnetics: Numerical methods; 0669 Electromagnetics: Scattering and diffraction

1. Introduction

[2] Method of moments (MOM) techniques have been widely used in electromagnetics to solve radiation and scattering problems. For perfect electric conductor (PEC) geometries a surface integral equation formulation is typically used, and a suitable geometry modeling scheme along with appropriate basis functions has been demonstrated to have significant effect on the accuracy of the solution [*Antilla and Alexopoulos*, 1994; *Song and Chew*, 1995].

[3] Several methods have been used to formulate scattering and radiation problems involving dielectric materials. The finite element method (FEM), along with various mesh truncation schemes [*Volakis et al.*, 1998], is one of the most commonly used approaches. Among these FEMs the finite element boundary integral (FE-BI) method [*Volakis et al.*, 1998] provides an exact means of truncating the FEM mesh, hence keeping the FEM domain small. Keeping the FEM domain small is crucial in numerical simulations since the FEM is prone to error propagation. The necessity of using suitable geometry modeling schemes and basis functions in the FE-BI formulation has also been demonstrated to be important, both in terms of solution accuracy and in terms of convergence. When dealing with homogeneous regions, a surface integral equation formulation can be used [*Poggio and Miller*, 1973]. However, for regions with varying material properties a volume integral equation must be employed [*Livesay and Chen*, 1974; *Schaubert et al.*, 1984]. *Livesay and Chen* [1974] used cubic elements in this context, and tetrahedral elements were used by *Schaubert et al.* [1984]. For curved geometries, tetrahedral elements are suitable because of their flexibility in modeling. However, when dealing with thin layers, hexahedral elements are more suitable since they avoid elongated tetrahedra, which lead to ill-conditioned matrix systems.

[4] Also, so far, direct volume integral equations (VIEs) have not been exploited because of their excessive CPU and memory requirements. Nevertheless, the recent introduction of fast methods [*Coifman et al.*, 1993] is beginning to make VIE solutions more practical. In this paper, we consider direct VIE solutions of electromagnetics problems using curvilinear hexahedra, which are particularly suited for thin layers and curvilinear volumes.

2. Volume Integral Equation Formulation and Solution

[5] Referring to Figure 1, the electric field integral equation for modeling the volume of a dielectric structure is given by

$$\mathbf{E}(\mathbf{r}) = \mathbf{E}_{\mathrm{inc}}(\mathbf{r}) + \int_v dv' \bar{\mathbf{G}}(\mathbf{r}, \mathbf{r}') \left[k^2(\mathbf{r}') - k_0^2\right] \mathbf{E}(\mathbf{r}'). \quad (1)$$

Here, v denotes the domain of the dielectric volume, $\mathbf{E}_{\mathrm{inc}}$ is the incident or excitation electric field, $k(\mathbf{r}) = k_0\sqrt{\varepsilon_r(\mathbf{r})}$ is the wave number inside the inhomogeneous

0048-6604/02/2000RS002597

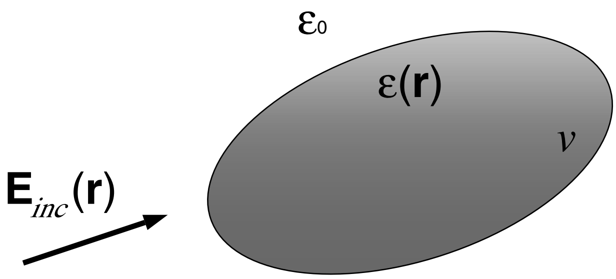

Figure 1. Dielectric structure illuminated by an incident field.

medium, r is the position vector, k_0 is the free space wave number, $\varepsilon_r(\mathbf{r})$ is the relative dielectric constant, and

$$\bar{\mathbf{G}}(\mathbf{r},\mathbf{r}') = \left[\bar{\mathbf{I}} + \frac{1}{k_0^2}\nabla\nabla\right] g(\mathbf{r},\mathbf{r}') \tag{2}$$

is the dyadic Green's function, where $g(\mathbf{r},\mathbf{r}') = e^{ik_0|\mathbf{r}-\mathbf{r}'|}/|\mathbf{r}-\mathbf{r}'|$ (an $e^{-i\omega t}$ time dependence is assumed and suppressed). To solve for $\mathbf{E}$, we proceed to discretize the volume v using hexahedra and introduce the expansion

$$\mathbf{E}(\mathbf{r}) \approx \sum_{i=1}^{N} a_i \mathbf{e}_i(\mathbf{r}), \tag{3}$$

where a_i are the unknown expansion coefficients, N denotes the number of basis functions used to discretize the domain, and $\mathbf{e}_i(\mathbf{r})$ are the basis functions defined within the hexahedra and are given in section 3. As noted above, we employ the higher-order hexahedral elements reported by *Antilla and Alexopoulos* [1994].

[6] Substituting (3) into (1) and employing Galerkin's testing, we obtain the matrix system $[Z][a] = [b]$, with the elements of the impedance matrix given by

$$Z_{ji} = \left\langle \mathbf{e}_j(\mathbf{r}), \mathbf{e}_i(\mathbf{r})\right\rangle - \left\langle \mathbf{e}_j(\mathbf{r}), \int_v dv' \bar{\mathbf{G}}(\mathbf{r},\mathbf{r}') \cdot \left[k^2(\mathbf{r}') - k_0^2\right] \mathbf{e}_i(\mathbf{r}') \right\rangle. \tag{4}$$

Those of the excitation vector are $b_j = \langle \mathbf{e}_j(\mathbf{r}), \mathbf{E}_{\mathrm{inc}}(\mathbf{r})\rangle$. The inner product $\langle \mathbf{f}, \mathbf{g}\rangle$ is defined as

$$\langle \mathbf{f}, \mathbf{g}\rangle = \int_v \mathbf{f}\cdot\mathbf{g}\, dv. \tag{5}$$

Throughout this paper the dielectric parameters of each finite element are assumed to be constant. The evaluation of the self-cells of this matrix is discussed in Appendix A.

3. Geometry Discretization and Basis Functions

[7] In this section, we discuss details associated with the discretization of the volume geometry using hexahedra. Referring to Figure 2, any point inside the hexahedron is a parametric mapping of a corresponding point in a unit cube through the transformation

$$\mathbf{r}(u,v,w) = \sum_{i=0}^{2}\sum_{j=0}^{2}\sum_{k=0}^{2} \mathbf{r}_{ijk} L_{ijk}(u,v,w), \quad (u,v,w) \in ([0,1],[0,1],[0,1]), \tag{6}$$

where $\mathbf{r}_{ijk}$ define the 27 points of the hexahedron and $L_{ijk}(u, v, w)$ are the quadratic Lagrange interpolation functions in three parameters (u, v, w). These coefficients can be constructed using the 27 constraints: $\mathbf{r}(0.0, 0.0, 0.0) = \mathbf{r}_{000}$, $\mathbf{r}(0.5, 0.0, 0.0) = \mathbf{r}_{100}$, $\mathbf{r}(1.0, 0.0, 0.0) = \mathbf{r}_{200}, \ldots, \mathbf{r}(1.0, 1.0, 1.0) = \mathbf{r}_{222}$.

[8] The set of basis functions used in this work are edge-based functions defined in curved hexahedra and are defined in terms of the covariant unitary vectors. The four basis functions associated with the edges parallel to the parametric direction u have the form

$$\mathbf{e}^{(u)}[\mathbf{r}(u,v,w)] = \frac{1}{\sqrt{G}} \begin{Bmatrix} 1-v \\ v \end{Bmatrix} \begin{Bmatrix} 1-w \\ w \end{Bmatrix} \frac{\partial \mathbf{r}}{\partial u}. \tag{7}$$

Similarly, for the edges in the v and w parametric directions, the basis functions are defined by

$$\mathbf{e}^{(v)}[\mathbf{r}(u,v,w)] = \frac{1}{\sqrt{G}} \begin{Bmatrix} 1-u \\ u \end{Bmatrix} \begin{Bmatrix} 1-w \\ w \end{Bmatrix} \frac{\partial \mathbf{r}}{\partial v}, \tag{8}$$

$$\mathbf{e}^{(w)}[\mathbf{r}(u,v,w)] = \frac{1}{\sqrt{G}} \begin{Bmatrix} 1-u \\ u \end{Bmatrix} \begin{Bmatrix} 1-v \\ v \end{Bmatrix} \frac{\partial \mathbf{r}}{\partial w}. \tag{9}$$

The curly brackets above imply that any of the two choices enclosed in the brackets can be selected. Thus each of (7), (8), or (9) represent four possible choices for the basis functions. The appropriate choice depends on the edge being considered. The determinant of the parametric transformation (6) is given by

$$G = \begin{vmatrix} g_{uu} & g_{uv} & g_{uw} \\ g_{vu} & g_{vv} & g_{vw} \\ g_{wu} & g_{wv} & g_{ww} \end{vmatrix}, \tag{10}$$

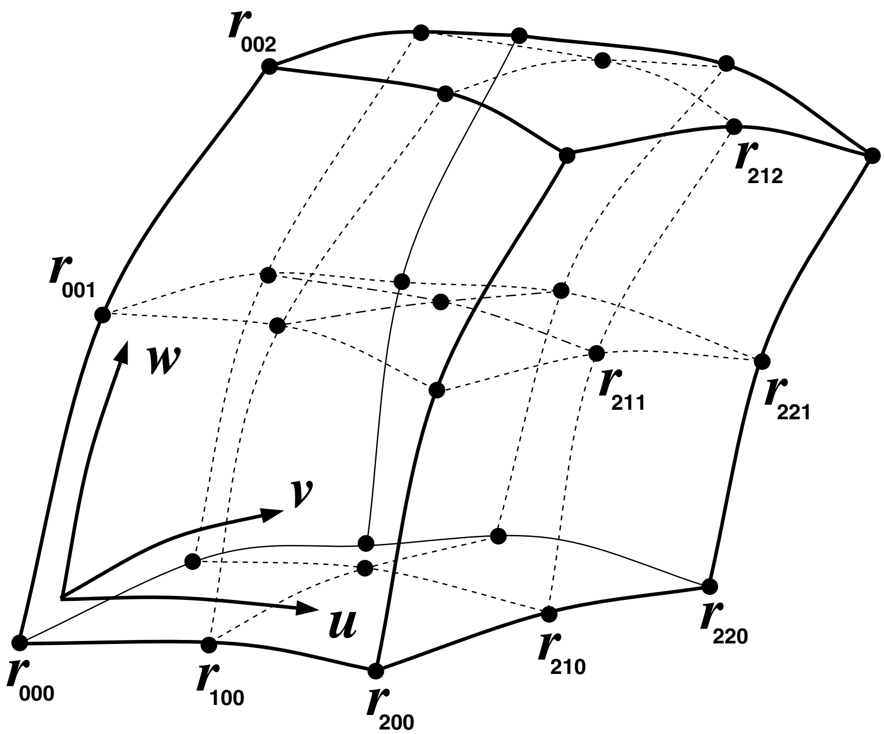

Figure 2. Curvilinear hexahedral element.

in which

$$g_{\eta\xi} = \frac{\partial \mathbf{r}}{\partial \eta} \cdot \frac{\partial \mathbf{r}}{\partial \xi}. \tag{11}$$

Here, η and ξ represent any of the parameters u, v, and w. Expressions (7)–(9) represent a set of 12 basis functions for each hexahedron. However, the total number of unknowns for a given tessellation is determined by the number of edges in the mesh. This is because the coefficients of the basis functions in adjoining elements sharing the same edge will be identical. Thus $\mathbf{e}_i$ in (3) will be some combination of (7)–(9) from different hexahedra as determined by the impedance matrix assembly process.

[9] The basis functions defined here are slightly different from those given by *Crowley et al.* [1988]. They are defined in terms of covariant unitary basis vectors, whereas the basis functions given by *Crowley et al.* [1988] are defined using contravariant unitary basis vectors. Being defined by covariant basis vectors, they have the advantages of having continuous tangential components across common faces of neighboring hexahedra, and have zero divergence inside the hexahedron. The latter property is not shared by the basis functions given by *Crowley et al.* [1988]. Both of these properties must be satisfied by the electric field intensity **E**.

4. Numerical Results

[10] Two examples were used to validate the above VIE solution. For both examples, the conjugate gradient squared (CGS) solver was used to solve the matrix system. We remark that since (1) is a second kind integral equation, CGS converged rather rapidly (in 10 iterations for 300 unknowns with a 10^{-4} residual).

[11] The first geometry considered is a dielectric sphere of radius 0.2 λ having ε_r = 2.592. Figure 3 shows the computed bistatic radar cross section (RCS) using our MOM formulation and Mie series. As seen, the VIE provides excellent agreement between the computed and analytical data. More importantly, this level of accuracy is achieved using a fairly low sampling because of the conformality of the curved hexahedra. The convergence of the solution can be observed by comparing the results of two different discretizations (for N = 300 and N = 882).

[12] Our second geometry is a spherical shell. The dielectric constant of the shell is ε_r = 1.75 + 0.3i, the

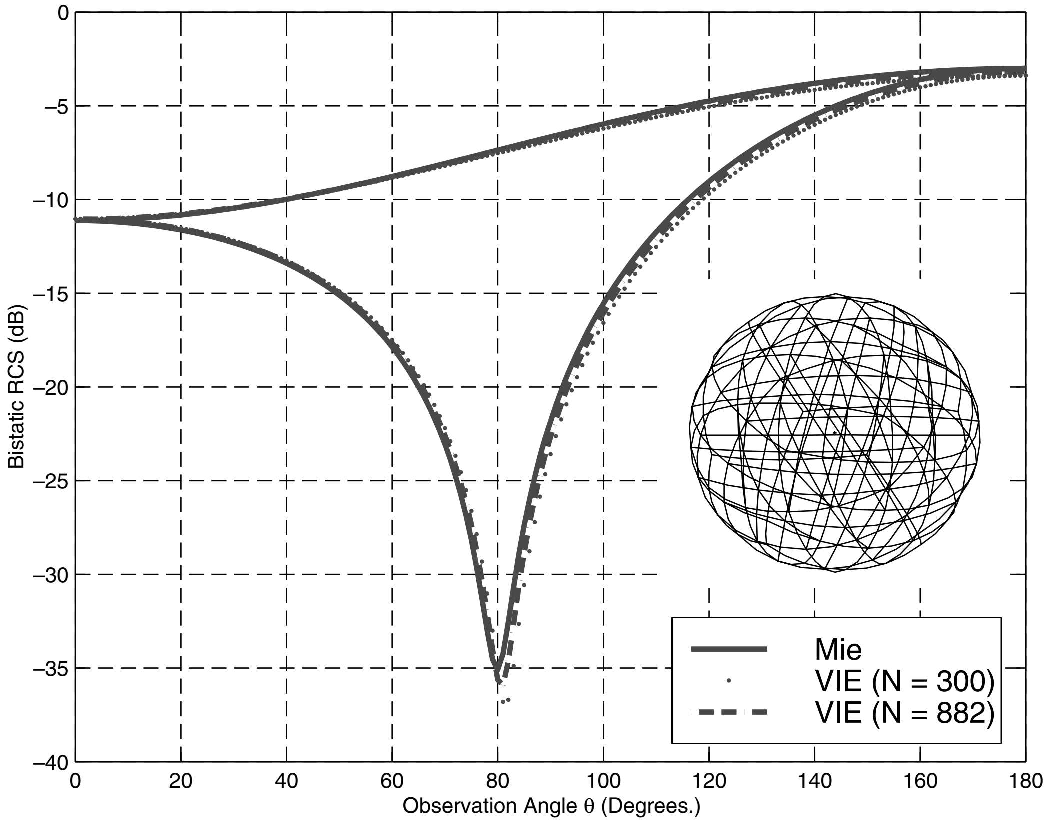

Figure 3. Bistatic RCS of a 0.2λ radius dielectric sphere (ε_r = 2.592) using VIE and Mie solutions.

outer radius is 0.2λ, and the shell thickness is 0.02λ. From Figure 4 it can be seen that the VIE solution curve is in very good agreement with the analytical solution.

[13] The VIE converged fast (in 10 iterations) as compared to a FE-BI solution (in 160 iterations) using the same hexahedral finite elements. In terms of CPU time for solving the same problem, the VIE outperforms the FE-BI by a factor of 10. An additional advantage of the VIE is its inherent property of being free of spurious resonances. In terms of accuracy, when the same geometrical model of the sphere (using 64 hexahedra) is used, the maximum RCS error in the VIE solution is 4.8%, whereas that for the FE-BI solution is 9.4%. Basically, FE-BI needed much finer discretization (216 elements and 1314 unknowns) to achieve a 4.6% error. It must also be noted that, to achieve this level of accuracy, a much higher discretization density would be required when a low-order geometry modeling scheme is used. Here, the percent error is computed by

$$\text{error} = \frac{||\text{computed}| - |\text{reference}||}{|\text{reference}|} \times 100\%. \qquad (12)$$

5. Conclusions

[14] A general volume integral equation formulation was presented for electromagnetic scattering using a new class of elements suited for modeling inhomogeneous scatterers. Higher-order finite elements and conformal basis functions were used to model the volume. Also, a new annihilation technique was described for evaluating the self-cell impedance matrix elements. Based on the considered geometries, the solution of the resulting matrix system was shown to provide more accurate results and faster convergence than those based on partial differential equation methods.

Appendix A: Evaluation of Self Term in the Impedance Matrix

[15] The matrix elements in (4) can be rewritten as

$$Z_{ji} = \langle \mathbf{e}_j(\mathbf{r}), \mathbf{e}_i(\mathbf{r}) \rangle - \langle \mathbf{e}_j(\mathbf{r}), \mathbf{I}_1(\mathbf{r}) \rangle + \frac{1}{k_0^2} \langle \mathbf{e}_j(\mathbf{r}), \mathbf{I}_2(\mathbf{r}) \rangle, \qquad (13)$$

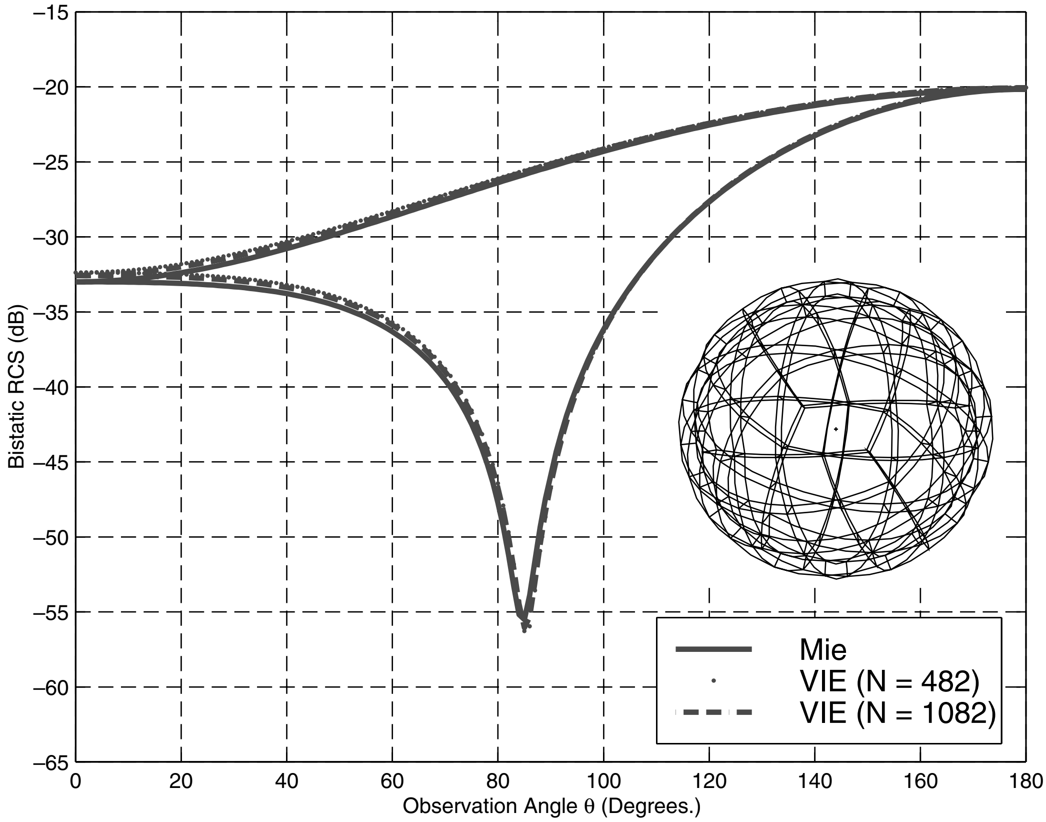

Figure 4. Bistatic RCS of a dielectric spherical shell ($\varepsilon_r = 1.75 + 0.3i$, outer radius is 0.2λ, and thickness is 0.02λ).

where

$$\mathbf{I}_1(\mathbf{r}) = \int_v dv' g(\mathbf{r}, \mathbf{r}')\left[k^2(\mathbf{r}') - k_0^2\right]\mathbf{e}_i(\mathbf{r}'), \tag{14}$$

$$\mathbf{I}_2(\mathbf{r}) = \nabla \int_v dv' \nabla g(\mathbf{r}, \mathbf{r}') \cdot \left[k^2(\mathbf{r}') - k_0^2\right]\mathbf{e}_i(\mathbf{r}'). \tag{15}$$

To deal with the $1/|\mathbf{r} - \mathbf{r}'|^3$ singularity in $\mathbf{I}_2(\mathbf{r})$, we proceed as usual by transferring the ∇ operator to the testing function. We have

$$\begin{aligned}
\int_v dv \mathbf{e}_j(\mathbf{r}) \cdot \mathbf{I}_2(\mathbf{r})
&= \int_v dv \mathbf{e}_j(\mathbf{r}) \cdot \nabla \int_v dv' \nabla g(\mathbf{r}, \mathbf{r}') \cdot \left[k^2(\mathbf{r}') - k_0^2\right]\mathbf{e}_i(\mathbf{r}') \\
&= \int_v dv \nabla \cdot \left\{\mathbf{e}_j(\mathbf{r}) \int_v dv' \nabla g(\mathbf{r}, \mathbf{r}') \cdot \left[k^2(\mathbf{r}') - k_0^2\right]\mathbf{e}_i(\mathbf{r}')\right\} \\
&\quad - \int_v dv \{\nabla \cdot \mathbf{e}_j(\mathbf{r})\} \int_v dv' \nabla g(\mathbf{r}, \mathbf{r}') \cdot \left[k^2(\mathbf{r}') - k_0^2\right]\mathbf{e}_i(\mathbf{r}') \\
&= \oint d\mathbf{s} \cdot \left\{\mathbf{e}_j(\mathbf{r}) \int_v dv' \nabla g(\mathbf{r}, \mathbf{r}') \cdot \left[k^2(\mathbf{r}') - k_0^2\right]\mathbf{e}_i(\mathbf{r}')\right\} \\
&\quad - \int_v dv \nabla \cdot \mathbf{e}_j(\mathbf{r}) \int_v dv' \nabla g(\mathbf{r}, \mathbf{r}') \cdot \left[k^2(\mathbf{r}') - k_0^2\right]\mathbf{e}_i(\mathbf{r}'),
\end{aligned} \tag{16}$$

where s denotes the surface enclosing v. The source (primed) integral in (16) can be further rewritten as

$$\begin{aligned}
&\int_v dv' \nabla g(\mathbf{r}, \mathbf{r}') \cdot \left[k^2(\mathbf{r}') - k_0^2\right]\mathbf{e}_i(\mathbf{r}') \\
&= -\int_v dv' \nabla' g(\mathbf{r}, \mathbf{r}') \cdot \left[k^2(\mathbf{r}') - k_0^2\right]\mathbf{e}_i(\mathbf{r}') \\
&= -\int_v dv' \nabla' \cdot \left\{g(\mathbf{r}, \mathbf{r}') \cdot \left[k^2(\mathbf{r}') - k_0^2\right]\mathbf{e}_i(\mathbf{r}')\right\} \\
&\quad + \int_v dv' g(\mathbf{r}, \mathbf{r}') \nabla' \cdot \left\{\left[k^2(\mathbf{r}') - k_0^2\right]\mathbf{e}_i(\mathbf{r}')\right\} \\
&= -\oint_s d\mathbf{s}' \cdot g(\mathbf{r}, \mathbf{r}')\left[k^2(\mathbf{r}') - k_0^2\right]\mathbf{e}_i(\mathbf{r}') \\
&\quad + \int_v dv' g(\mathbf{r}, \mathbf{r}') \nabla' \cdot \left\{\left[k^2(\mathbf{r}') - k_0^2\right]\mathbf{e}_i(\mathbf{r}')\right\}.
\end{aligned} \tag{17}$$

[16] The above integrals are not improper, but nevertheless, their numerical integration must be carefully

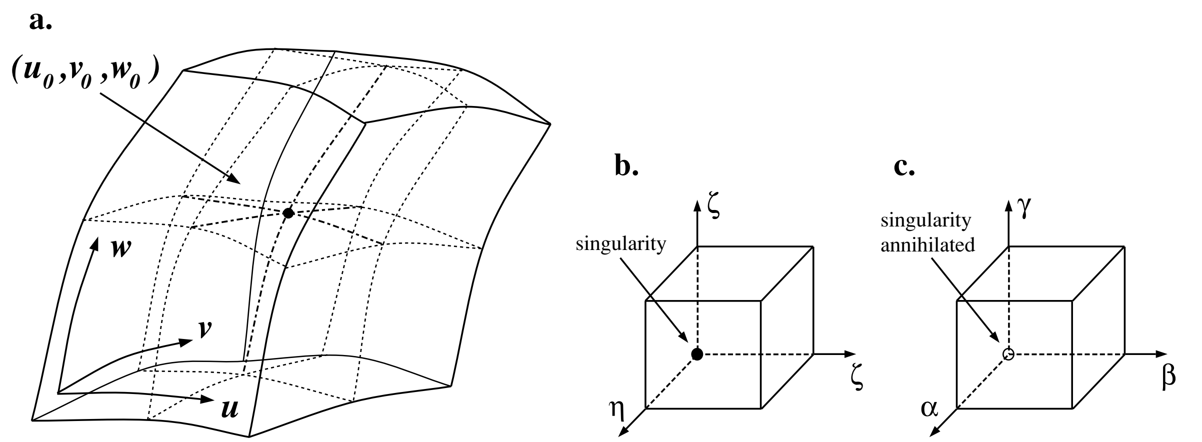

Figure 5. (a) Hexahedron in real space, (b) auxiliary parametric space, and (c) integration space.

done because of the first-order singularity of the Green's function. To evaluate the singular source integrals in (17), we herewith employ an annihilation technique that converts the singular integrands from the original (u, v, w) parametric space to smooth, nonsingular integrands on an auxiliary (α, β, γ) parametric space. To illustrate this, let us consider the source term volume integral in (17). First, we recast it in the (u, v, w) space as

$$I = \int_0^1 \int_0^1 \int_0^1 g(\mathbf{r}, \mathbf{r}')\nabla' \cdot \left\{ \left[k^2(\mathbf{r}') - k_0^2\right] \mathbf{e}_i(\mathbf{r}')\right\} \sqrt{G} du dv dw. \tag{18}$$

For further discussion, we conveniently rewrite (18) in a more general form as a ratio of two well-behaved functions in the (u, v, w) space

$$I = \int_0^1 \int_0^1 \int_0^1 \frac{f(u_0, v_0, w_0, u, v, w)}{g(u_0, v_0, w_0, u, v, w)} du dv dw, \tag{19}$$

where $g(u_0, v_0, w_0, u, v, w) = 0$ when $(u, v, w) = (u_0, v_0, w_0)$ and $f(u_0, v_0, w_0, u, v, w)$ is well behaved at the same point. We note that in (19) the original observation point has been mapped to (u_0, v_0, w_0).

[17] The next step in the annihilation process is to divide the unit cube into eight quadrants using the three planes defined by $u = u_0$, $v = v_0$, and $w = w_0$ (see Figure 5a). When these quadrants are considered separately, the original singularity now appears at a vertex of each of the eight quadrants. For integration we next proceed to map each of the eight quadrants to a unit cube in the (η, ζ, ξ) parametric space as shown in Figure 5b. We need to again be careful to choose our transformations so that the singularity for one of the vertices of each quadrant appears at the origin of the (η, ζ, ξ) space. For example, the transformation to map one of the quadrants defined by ($u_0 < u < 1$), ($0 < v < v_0$), ($w_0 < w < 1$) is

$$\begin{aligned} u &= (1 - u_0)\eta + u_0, \\ v &= v_0(1 - \zeta), \\ w &= (1 - w_0)\xi + w_0. \end{aligned} \tag{20}$$

Similar transformations must be used for the other seven quadrants.

[18] Using this eight-quadrant decomposition, the integral (19) can be written as

$$I = \sum_{i=1}^{8} \int_0^1 \int_0^1 \int_0^1 \frac{f_i(\eta, \zeta, \xi)}{g_i(\eta, \zeta, \xi)} J_i(\eta, \zeta, \xi) d\eta d\zeta d\xi, \tag{21}$$

where $J_i(\eta, \zeta, \xi)$ are the Jacobians of the transformations for each quadrant and f_i and g_i are the portions of the original f and g that fall in respective quadrants. We should remark that f_i, g_i, and J_i do depend on (u_0, v_0, w_0), but this dependence has been suppressed. Also, since the transformations used to map (η, ζ, ξ) to (u, v, w) are simple scaling transformations, the Jacobians $J_i(\eta, \zeta, \xi)$ are constants. For the example given in (20) the Jacobian is simply $J_i = (1 - u_0)(-v_0)(1 - w_0)$.

[19] A final step for integration is to propose another parametric transformation whose Jacobian has a zero (of order equal to or higher than that of g) at the origin of the (η, ζ, ξ) space (Figure 5c). One such transformation is

$$\begin{aligned} \eta &= \alpha^3, \\ \zeta &= \beta^3, \\ \xi &= \gamma^3, \end{aligned} \tag{22}$$

and we note that a third-order transformation is used for sufficient smoothness of the integrand in the (α, β, γ) space. Doing this transformation allows us to rewrite the integral (21) as

$$I = \sum_{i=1}^{8} \int_0^1 \int_0^1 \int_0^1 \frac{f_i(\alpha,\beta,\gamma)}{g_i(\alpha,\beta,\gamma)} J_i\, j(\alpha,\beta,\gamma) d\alpha d\beta d\gamma. \tag{23}$$

In this, $j(\alpha, \beta, \gamma) = 27\alpha^2\beta^2\gamma^2$ is the Jacobian of the (η, ζ, ξ) to (α, β, γ) transformation. Since the Jacobian has a second-order zero at the origin of the (α, β, γ) space, it serves to annihilate the singularity $1/g_i(\alpha, \beta, \gamma)$ in each of the eight quadrants. Thus (23) has a nonsingular integrand and can be evaluated numerically using a sufficient order quadrature rule (e.g., Gaussian quadrature).

[20] A similar integration procedure can be applied to evaluate the surface source integral in (17), considering each of the six faces of the source hexahedron separately.

[21] **Acknowledgments.** This work was supported by NPACI.

References

Antilla, G. E., and N. G. Alexopoulos, Scattering from complex 3D geometries by a curvilinear hybrid finite element-integral equation approach, *J. Opt. Soc. Am. A Opt. Image Sci.*, *11*(4), 1445–1457, 1994.

Coifman, R., V. Rokhlin, and S. Wandzura, The fast multipole method for the wave equation: A pedestrian prescription, *IEEE Antennas Propag. Mag.*, *35*, 7–12, 1993.

Crowley, C. W., P. P. Silvester, and H. Hurwitz Jr., Covariant projection elements for 3D vector field problems, *IEEE Trans. Magn.*, *24*(1), 397–400, 1988.

Livesay, D. E., and K. Chen, Electromagnetic fields induced inside arbitrarily shaped biological bodies, *IEEE Trans. Microwave Theory Tech.*, *MTT-22*, 1273–1280, 1974.

Poggio, A. J., and E. K. Miller, Integral equation solutions of three dimensional scattering problems, in *Computer Techniques for Electromagnetics*, pp. 159–264, Permagon, New York, 1973.

Schaubert, D. H., D. R. Wilton, and A. W. Glisson, A tetrahedral modeling method for electromagnetic scattering by arbitrarily shaped inhomogeneous dielectric bodies, *IEEE Trans. Antennas Propag.*, *AP-32*(1), 77–85, 1984.

Song, J. M., and W. C. Chew, Moment method solution using parametric geometry, *J. Electromagn. Waves Appl.*, *9*, 71–83, 1995.

Volakis, J. L., A. Chatterjee, and L. C. Kempel, *Finite Element Methods for Electromagnetics*, IEEE Press, Piscataway, N. J., 1998.

K. Sertel and J. L. Volakis, Radiation Laboratory, Department of Electrical Engineering and Computer Science, University of Michigan, Ann Arbor, MI 48109-2122, USA. (ksertel@eecs.umich.edu; volakis@eecs.umich.edu)